GENERAL RELATIVISTIC HYDRODYNAMICS AND ACCRETION PHYSICS: A NUMERICAL APPROACH

John F. Hawley, Larry L. Smarr

Department of Astronomy, University of Illinois
Urbana, Illinois 61801

We describe a numerical approach to the equations of general relativistic hydrodynamics. A discussion of the development and use of our computer code to study axisymmetric accretion flows around black holes is featured. We outline the equations to be solved, the numerical techniques used and our code calibration "test bed." An illustrative accretion disk formation is presented.

1. INTRODUCTION

The accretion of matter into black holes is believed to play a vital role in many astrophysical situations. Such a process may very well power quasars, Seyfert galaxies and active galactic nuclei. Many fundamental questions regarding the accretion process have not been answered and can not be addressed with the techniques presently used. Progress will require investigating the dynamic evolution of these systems; the fully time-dependent equations will have to be solved. The approach we have selected to address some of the current theoretical questions is to use time explicit, Eulerian finite differencing to solve the dynamic axisymmetric equations of general relativistic hydrodynamics. To implement this approach we have written a computer code to investigate the behavior of fluid with angular momentum in the fixed Kerr metric. We have calibrated the code against our knowledge of the behavior of test particles and the hydrodynamics of highly idealized flows. However, in general, our results will involve phenomena which could not previously be examined, including shocks, vortical motions and the non-linear development of instabilities. This code a requisite first step towards

D. Bancel and M. Signore (eds.), Problems of Collapse and Numerical Relativity, 253–269.
© 1984 by D. Reidel Publishing Company.

solving the more general and complicated problems involving the magnetohydrodynamic equations, dynamic viscosity and radiation transport. As the first step, we will uncover the dominant hydrodynamical effects through a study of the motion of a perfect fluid in the near hole region, thereby mapping out the phenomenology of a portion of solution space.

This paper will review our work in the subject of general relativistic hydrodynamics, briefly describing the equations and the numerical approach we use to solve them. This is in part an index to the more detailed discussion given in Hawley, Smarr and Wilson (1-2, papers I and II). As an example, we include a discussion of a thick disk formation calculation.

2. EQUATIONS

We begin by considering both the fundamental and some derived variables of relativistic hydrodynamics as they will be used in the code. The fluid we wish to study will have a 4-velocity- U^μ (μ = 0,1,2,3) at each event, which is the 4-velocity of an observer comoving with the fluid at that point. Express the 4-velocity in units of the speed of light c. At this same event we require three scalar functions. The first of these is the baryon rest mass density $\rho(gm/cm^3)$. Consider only a one particle fluid and allow no nuclear reactions. This allows the baryon mass density and the baryon number density (often written "n" by many authors) to be used interchangeably. The other scalar functions are the specific internal energy ε (ergs/gm) - the temperature in a perfect gas - and the isotropic pressure P (units of $\rho\varepsilon$ - energy density). The pressure P is connected to the other variables by an equation of state $P = P(\rho,\varepsilon)$. We will often wish to consider the ideal gas equation of state given by $P = \rho\varepsilon(\Gamma - 1)$, where Γ is the ideal gas adiabatic exponent. The relativistic enthalpy is written $h = 1 + \varepsilon + P/\rho$. The quantity ρh is the total inertia-carrying mass energy. Note that for the ideal gas equations of state $\rho h = \rho(1+\Gamma\varepsilon)$. For a comparison of our notation to that of other authors, see Smarr, Taubes, and Wilson (3).

We use geometric units in which G = c = M = 1 (M = black hole mass). To convert back to conventional units simply multiply the geometric value by dimensionally correct factors of G, c, and M. Note that since the mass of the accreting fluid does not contribute to the dynamics, the density is essentially scale-free. To describe an astrophysical problem in conventional units, relate the geometric density and energy to a reference value, such as the matter density and energy at infinity.

Next, let us define the important relativity variables. First the "relativistic gamma", often written γ, is written here as W:

$$W = (1 - V^\mu V_\mu)^{-1/2} \quad . \tag{1a}$$

V^μ shall be referred to as the "transport velocity"

$$U^\mu = \frac{W}{\alpha} V^\mu . \tag{1b}$$

Next consider the "lapse function" $\alpha = (-g^{tt})^{-1/2}$. Proper time along the unit normal from one spacelike hypersurface at coordinate time t to a second such surface at coordinate time t + dt is given by $d\tau = \alpha dt$. Together α and W make up respectively the total "gravitational" and "Doppler" redshift factor $W/\alpha = U^t$, the contravariant time component of the fluid four-velocity. A complete discussion of the lapse function and the "3 + 1" coordinate slicing is given by York (4).

Finally there are the components of the black hole metric g. The metric is assumed to be stationary and axisymmetric. It is completely specified by the mass of the hole M, and its angular momentum per unit mass a (Kerr geometry - assume charge Q on hole is zero). Express the metric in Schwarzschild-like (Boyer-Lindquist) coordinates. The line element is:

$$ds^2 = g_{tt}dt^2 + 2g_{t\phi}\, dtd\phi + g_{\phi\phi}d\phi^2 + g_{rr}dr^2 + g_{\theta\theta}d\theta^2 \tag{2}$$

Choose the spacelike signature (-,+,+,+).

The square root of the determinant of the 4-metric is written $\sqrt{-g}$. The square root of the determinant of the 3-metric is written $\sqrt{\gamma}$. The two are related by the lapse function:

$$\sqrt{-g} = \alpha\sqrt{\gamma} \tag{3}$$

Use the usual forms for derivatives. The covariant derivative is signified by a semicolon or a "del" operator with a greek index, i.e.

$$\nabla_\beta T^{\alpha\beta} = T^{\alpha\beta}{}_{;\beta} \tag{4}$$

signifies a covariant derivative with respect to β. Similarly the ordinary flat-space derivative is signified with a comma or a latin index.

These variables give the complete state of a uniform composition fluid system with no magnetic fields. Now assemble the equations which determine the evolution of such a fluid system. First there is the normalization of the four velocity:

$$U^\mu U_\mu = -1 \tag{5}$$

Next there are two fundamental conservation laws. These are 1) the conservation of baryon number

$$\nabla^\mu(\rho U_\mu) = 0 \tag{6}$$

and 2) the conservation of stress-energy:

$$\nabla_\mu(T^{\mu\nu}) = 0 \tag{7}$$

The tensor $T^{\mu\nu}$ is the stress-energy tensor. This second conservation law can be broken into two familiar forms: the conservation of energy

$$U^\mu \nabla^\nu T_{\mu\nu} = 0 \tag{8}$$

and the conservation of momentum

$$h_{\gamma\mu} \nabla_\nu T^{\mu\nu} = 0 \tag{9}$$

where $h_{\gamma\mu}$ is the spatial projection (into the fluid rest frame) tensor defined by

$$h_{\gamma\mu} = U_\gamma U_\mu + g_{\gamma\mu} \tag{10}$$

In the present analysis we are simplifying our system of equations to deal only with the perfect fluid stress-energy tensor:

$$T^{\mu\nu} = \rho h U^\mu U^\nu + P g^{\mu\nu} \tag{11}$$

With this we can write the perfect fluid equations of hydrodynamics in the form in which they will be studied numerically (5). The law of baryon conservation can be written

$$\frac{1}{\sqrt{-g}} \partial_\mu (\rho\sqrt{-g}\, U^\mu) = 0 \tag{12}$$

The metric is time independent by assumption. Now use the variable V^μ as defined in equation (1). This V^μ is the "transport velocity" of the fluid as measured by the observer at rest with respect to the coordinate grid points. Using this definition, write

$$\frac{1}{\sqrt{\gamma}} \partial_\mu (\rho\sqrt{\gamma}\, W V^\mu) = 0 \tag{13}$$

Now define $D = \rho W$ and obtain

$$\partial_t(D) + \frac{1}{\sqrt{\gamma}} \partial_i (D\sqrt{\gamma}\, V^i) = 0 \tag{14}$$

The energy equation is dealt with in a similar manner. Begin with

$$U^\nu(\nabla^\mu(\rho h U_\mu U_\nu) + \nabla_\nu P) = 0 \tag{15}$$

Remove the term $\nabla^\mu(\rho U_\mu)$ using baryon conservation; the remaining terms can be simplified to

$$\nabla^{\mu}(\rho\varepsilon U_{\mu}) + P\nabla^{\mu}U_{\mu} = 0 \tag{16}$$

Now define $E = \rho\varepsilon W$ to obtain

$$\partial_t E + \frac{1}{\sqrt{\gamma}}\partial_i(E\sqrt{\gamma}\, V^i) + P\partial_t(W) + \frac{P}{\sqrt{\gamma}}\partial_i\,(W\sqrt{\gamma}\, V^i) = 0 \tag{17}$$

For momentum conservation take the divergence of the stress-energy

$$\nabla_{\mu}\,(\rho h U^{\mu}U_{\nu} + P g^{\mu}{}_{\nu}) = 0 \tag{18}$$

and use the definition $S_{\nu} = \rho h W U_{\nu}$ to write

$$\frac{1}{\alpha\sqrt{\gamma}}\partial_{\mu}\,(\sqrt{\gamma}S_{\nu}V^{\mu}) - \Gamma^{\varepsilon}_{\mu\nu}\,(S_{\varepsilon}\frac{V^{\mu}}{\alpha}) - \nabla_{\nu}P = 0 \tag{19}$$

Note that $S^t = \rho h W U^t = \rho h W^2/\alpha$. Then

$$S_{\varepsilon}V^{\mu}/\alpha = S_{\varepsilon}S^{\mu}/\alpha S^t \tag{20}$$

which can be rewritten as

$$\Gamma^{\gamma}_{\mu\nu}\, S_{\gamma}S^{\mu} = \frac{1}{2}\, S^{\gamma}S^{\mu}\partial_{\nu}g_{\mu\gamma} = -\frac{1}{2}\, S_{\gamma}S_{\mu}\partial_{\nu}g^{\mu\gamma} \tag{21}$$

After taking the spatial component $\nu = j$, the momentum equation becomes

$$\partial_t(S_j) + \frac{1}{\sqrt{\gamma}}\partial_i\,(\sqrt{\gamma}\, S_j V^i) + \alpha\partial_j P + \frac{1}{2}\frac{S_{\gamma}S_{\mu}}{S^t}\partial_j g^{\gamma\mu} = 0 \tag{22}$$

Our perfect fluid equations are now complete.

3. NUMERICAL APPROACH

Having listed the equations describing the fluid system we now we briefly consider the general philosophy and technique of the approach we use to numerically study this system. The details of the finite differencing schemes are found in Paper II. Since we wish to study as wide a variety of physical systems as possible, the code must have sufficient generality and adaptability. Some of the fluid physics expected in accretion flows includes shocks, vortices, subsonic and supersonic flows, viscous effects, heating, cooling, angular momentum transport and magnetic fields. The physics involved in such phenomenon is idealized and included in the differential equations through the addition of new terms, e.g. viscosity terms. When such terms are to be included in the difference equations they should not require the development of an entirely new code. Rather the new work should augment and be built upon the old. Just as new physics is modeled by additional terms in the differential equations, we wish to include more physics by adding terms to the difference equations when possible.

Besides providing ease in applying new physics, a sufficiently adaptable code permits quick changes in finite difference methods. Not only does this allow for new or improved schemes to be immediately tested and used, but the comparison of results from schemes differing only by one technique or term is an excellent method of understanding exactly what features arise from the numerics and what represents physics.

These considerations require our 2-D code to be time explicit, that is each new time level is calculated using the values at the previous time level. The advantage of an explicit code is its simplicity. A time implicit code involves obtaining the simultaneous solutions of all equations for the next time level. The implicit difference equations are often difficult to formulate and code. In one spatial dimension, such codes are now in a state of mature development (6). However, in two spatial dimensions, such as we are studying, much more work and the use of supercomputers are required for time-implicit schemes.

An explicit code can use operator splitting (5) to solve one portion of the system of equations at a time. Finite difference methods are easily changed through the substitution of several lines of code; the whole program need not be rewritten. The major drawback to a time-explicit scheme is that the timestep is Courant-Friedrichs-Lewy (CFL) limited, and calculations involving long timescales (very many Δt) can be quite expensive to run. Nevertheless there are many problems which can be effectively investigated by an explicit code. Further, careful and extensive testing of explicit codes can lay the groundwork for future more accurate implicit codes.

We wish to study two-dimensional flows and such phenomenon as vortices; the code must therefore be Eulerian, i.e. fixed grid, rather than Lagrangian in which the grid is tied to fluid elements. In more than one dimension, grid distortion and the tangling of grid lines makes the Lagrangian scheme difficult to use. The main difference between the Eulerian and the Lagrangian approach is that an Eulerian scheme must calculate the transport of fluid in and out of the fixed grid zones. By making these "transport" terms as accurate as possible the disadvantages of the Eulerian scheme are minimized.

Shocks often play a key role in dynamic fluid flows. Such was the case in the first numerical study of 2-D black hole accretion (7) and now, as then, we choose to employ an artificial viscosity Q to deal with shock discontinuities. An artificial viscosity has two functions to perform. One is to permit resolution of the shock on a finite difference grid by being sufficiently dissipative so as to spread the otherwise discontinuous shock over several grid zones. The other function is to model the conversion of kinetic energy into internal energy. Von Neumann and Richtmyer (8) introduced a scalar Q which is added to the pressure in the stress-energy tensor; in this way it functions in the manner of a bulk viscosity term. We choose to use an

artificial viscosity to handle shock discontinuities because of its generality; it does a quite adequate job of modeling shocks and it does not add significant numerical dissipation to the equations in regions away from shocks; it is set equal to zero unless there is local compression. The use of Q is a general approach to the problem of shock dissipations making it easier to eventually employ an arbitrary equation of state and include some form of dynamic viscosity. This will be necessary to study the transport of angular momentum and heating in accretion disks.

4. CODE TESTS

Having developed a numerical approach, we implement our strategy through coding and compare results with intended goals by using checks for accuracy with known solutions, checks for self-consistency, and checks with physical intuition. Just as the experimental physicist must calibrate his laboratory equipment in order to interpret the results, the numerical theorist must similarly calibrate his code. This involves code testing. Such tests include studies of finite difference schemes in highly idealized, analytically clear-cut problems, e.g. shock tubes, advection of wave packets, simple accretion flows, etc. Particularly important are tests in the context of the problem you wish to solve; in our case this means obtaining the special accretion flows which are analytically solvable. The goal of these tests is to gauge the magnitude of diffusive error inherent in the difference scheme, insure self-consistency in the numerical formulation of the differential equations, demonstrate reproduction of analytic solutions and check on the numerical simulation of each piece of physics as modeled by the equations.

4.1 Shock Tubes

The first test problem is a series of one dimensional ideal fluid shock tubes involving both relativistic and non-relativistic fluid dynamics. Obtaining the analytic solution to a shock tube problem (see paper I) requires the use of 1) the characteristic curves of nonlinear waves and 2) conservation laws as realized in the shock jump conditions. The value of this problem as a code test arises from these same features. It can test 1) how well a finite difference scheme advects a nonlinear wave and 2) if conserved quantities are actually conserved. It can also show how well the shock dissipation mechanism (e.g. artificial viscosity Q) provides the correct jump across the shock. A comparison of several finite difference schemes on the same problem is especially useful for displaying features in a solution which arise solely due to the numerics, e.g. the relative amounts of artificial dissipation and post-shock oscillation. Such a comparison was performed by Sod (9).

We find (paper II) that with the "monotonic" schemes of van Leer (10) and Barton (11), we obtain results which are substantially improved over those obtained with either the non-monotonic schemes we tested or the schemes studied by Sod. Van Leer and Barton's schemes are second order and this reduces the diffusion error. The condition of monotonicity prevents the onset of the ringing often associated with higher order schemes.

4.2 Geodesic Infall

Next consider code tests in the context of fluid accretion onto black holes. One such accretion test is the spherical infall of dust, i.e. non-interacting test particles moving along geodesics. To model dust we require the fluid pressure to be negligible, i.e. $E/D \ll 1$. The dust is introduced, already in free fall from infinity, at the outer boundary of the grid and allowed to find a steady state solution. Analytic formulas yield exact values to all code variables; we use the analytic results to compare directly with the steady state numerical results at each point in the flow. From this we are able to gain insight into how well various portions of the full accretion code perform and what effects our boundary conditions may have.

4.3 Bondi Accretion

The next step in testing is to add a new dynamic element by allowing the ratio E/D to be non-negligible, thus making the pressure force a significant factor in determining the radial flow. The test problem is the general relativisitic Bondi accretion of fluid with non-zero pressure. Here we again test only radial differencing, but now all the hydrodynamic elements of the radial equations are dynamically important. The major new point here is the subsonic/supersonic transition which occurs at the analytically determinable sonic sphere around the black hole (see section Vb, paper I).

In both the Bondi and the dust tests, van Leer's monotonic scheme produced results accurate to a fraction of a percent at radii greater than about 4 M and to within a few percent very near to the horizon (see section IIIc(ii) in paper II). The calculation was performed on a coarse grid of 25 radial zones between $r = 2$ and 18 M. The non-monotonic second order scheme we tested showed evidence of ringing error and the first order donor cell scheme produced markedly inferior results. Inasmuch as the implementation of van Leer's monotonic scheme requires no more than a slight increase in programing effort and execution time, its use is highly recommended. The use of the first order donor cell scheme for production calculations can no longer be justified.

4.4 2-D Flow Tests

We now allow the fluid angular momentum as well as the pressure to be non-negligible, thus insuring new dynamical 2-D flows. The angular momentum provides centrifugal accelerations in the θ direction while the hot fluid provides a pressure gradient thus allowing vertical structure above the equatorial plane. In the radial testing, the code was required to evolve a set of initial conditions towards a known steady-state solution. This plan is more difficult to apply for 2-D flows since there are no simple analytic solutions for U^r and U^θ nonzero. However there is a steady state solution to the fluid equations which has a 2-D structure although there is no r or θ velocity. This is the hot, pressure-supported fat disk in which centripetal, pressure and gravitational accelerations are in balance at each point in the disk.

For test problems we will evolve disk models and fluid flows parameterized by constant angular momentum $\ell = -U_\phi/U_t$. There are three critial regimes of ℓ: $\ell > \ell_{ms}$, less than that of the marginally stable orbit around the black hole, $\ell > \ell_{mb}$, greater than the angular momentum of the marginally bound orbit, i.e. the minimum angular momentum which will still turn a particle falling from rest at infinity, and an intermediate angular momentum $\ell_{ms} < \ell < \ell_{mb}$. For more details on how an analytic disk is constructed and the relevant equations for disk structure, the reader is refered to paper I eqns. 85-95 and cited references.

Some of the fat disks - those with high angular momentum $\ell > \ell_{mb}$ - will be steady state; the code should evolve such models onto themselves. Any observed changes will provide an estimate of the numerical diffusion inherent in the code. In other cases where dynamic evolution is required, U^r and U^θ may be on the same order as U^ϕ. While the evolution from such models is not known in full analytic detail, certain flow patterns and features are expected. Observing the code evolution for such models provides an excellent check on the 2-D hydrodynamics. In addition these cases have aspects of interest in their own right. For models with $\ell < \ell_{ms}$ there will be no turning points in the orbits of the fluid. Any fluid with such an angular momentum will spiral into the hole. We can also evolve models in which fluid with angular momentum $\ell_{ms} < \ell < \ell_{mb}$ is allowed to flow onto the grid. Given this ℓ one can use the analytic model to predict turning points in the fluid orbits and the location of the stable circular orbit where a pressure and density maximum should form. We cannot expect to reproduce an analytic model exactly since the analytic case is not physical (for $\ell < \ell_{mb}$); it is based upon the idea that the disk will be static with $U^r = U^\theta = 0$. These conditions cannot hold for fluid with $\ell < \ell_{mb}$ and initial binding energy $hU_t = -1$. In this case the analytic model is only a guideline which can be used to gauge the results from the fully dynamic calculation.

We find that in the low angular momentum case, the fluid spirals smoothly into the hole. The angular momentum acts to funnel the flow towards the equator but does not prevent or otherwise disturb the accretion. In static disk tests with high angular momentum fluid, we evolved disks for up to six orbits at the pressure maximum. No systematic changes occured; the values of the fluid variables differed from the analytic by no more than 3% in the worst case and by less than a percent at the pressure maximum. Small changes in the fluid values are to be expected as the disk relaxes to its finite difference equilibrium configuration. Even on our coarse test grid (described below) this equilibrium is very close to the analytic one.

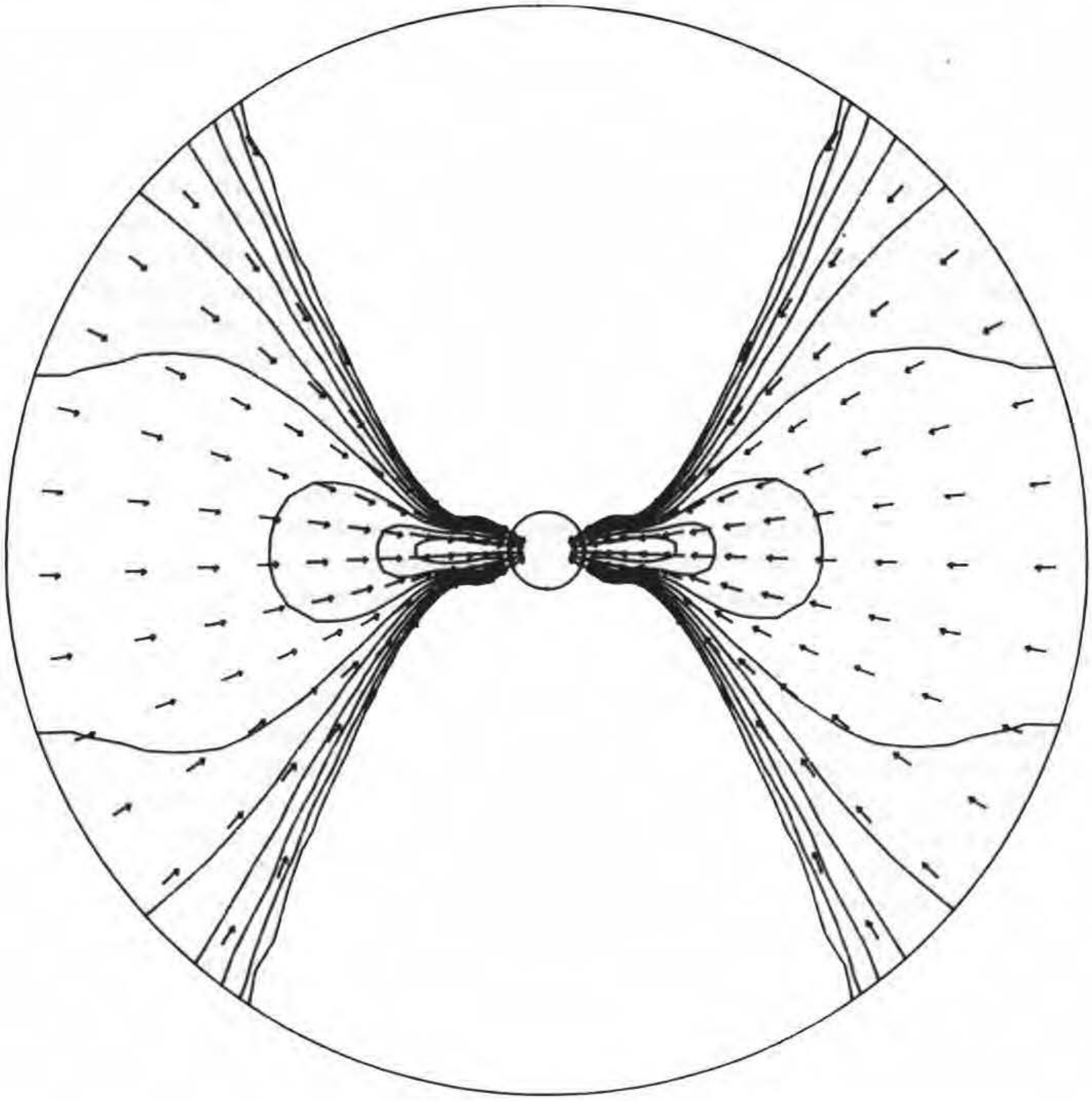


Figure One: Contours of logarithmic density and direction of fluid flow at time t = 130 M for the coarse grid disk formation calculation

5. DISK FORMATION

As an example of a test and an unknown accretion problem we present the dynamic formation of a thick accretion disk through the infall of fluid with ℓ = 3.77 (angular momentum between the "marginally stable" and "marginally bound" values). The outermost two radial grid zones are filled with fluid that has this value of ℓ. Gravitational and pressure gradient accelerations cause the fluid to fall towards the hole; a flux matching boundary condition resupplies the grid with additional fluid. We expect the infalling matter to fill up the potential surfaces predicted for a disk with this angular momentum. There will be an equatorial orbital turning point at the potential cusp located at r = 4.72 M and a pressure and density maximum at the stable circular orbit r = 8 M.

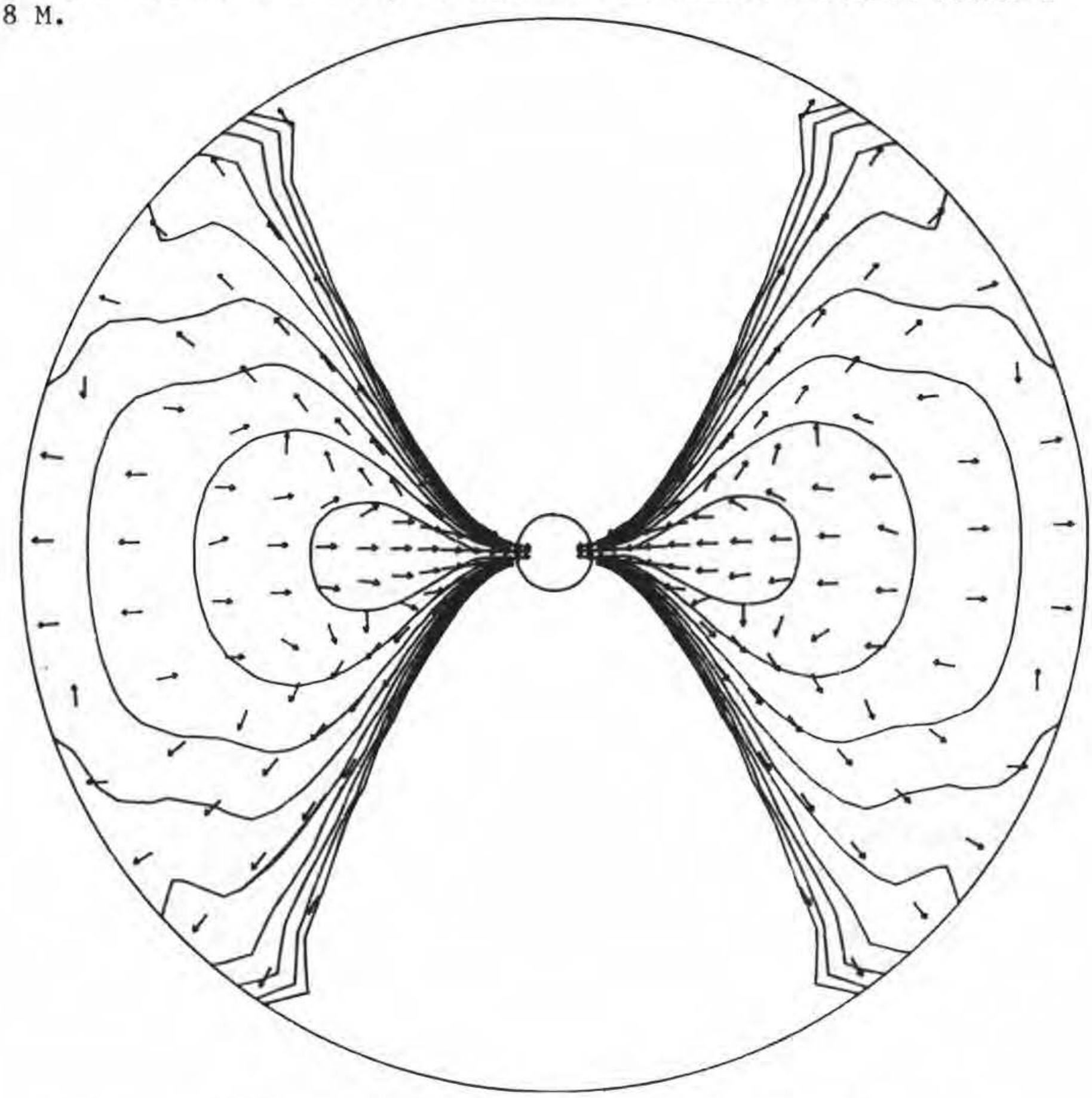


Figure two: Logarithmic density contours and fluid flow directions at t = 430 M for the coarse grid disk formation calculation

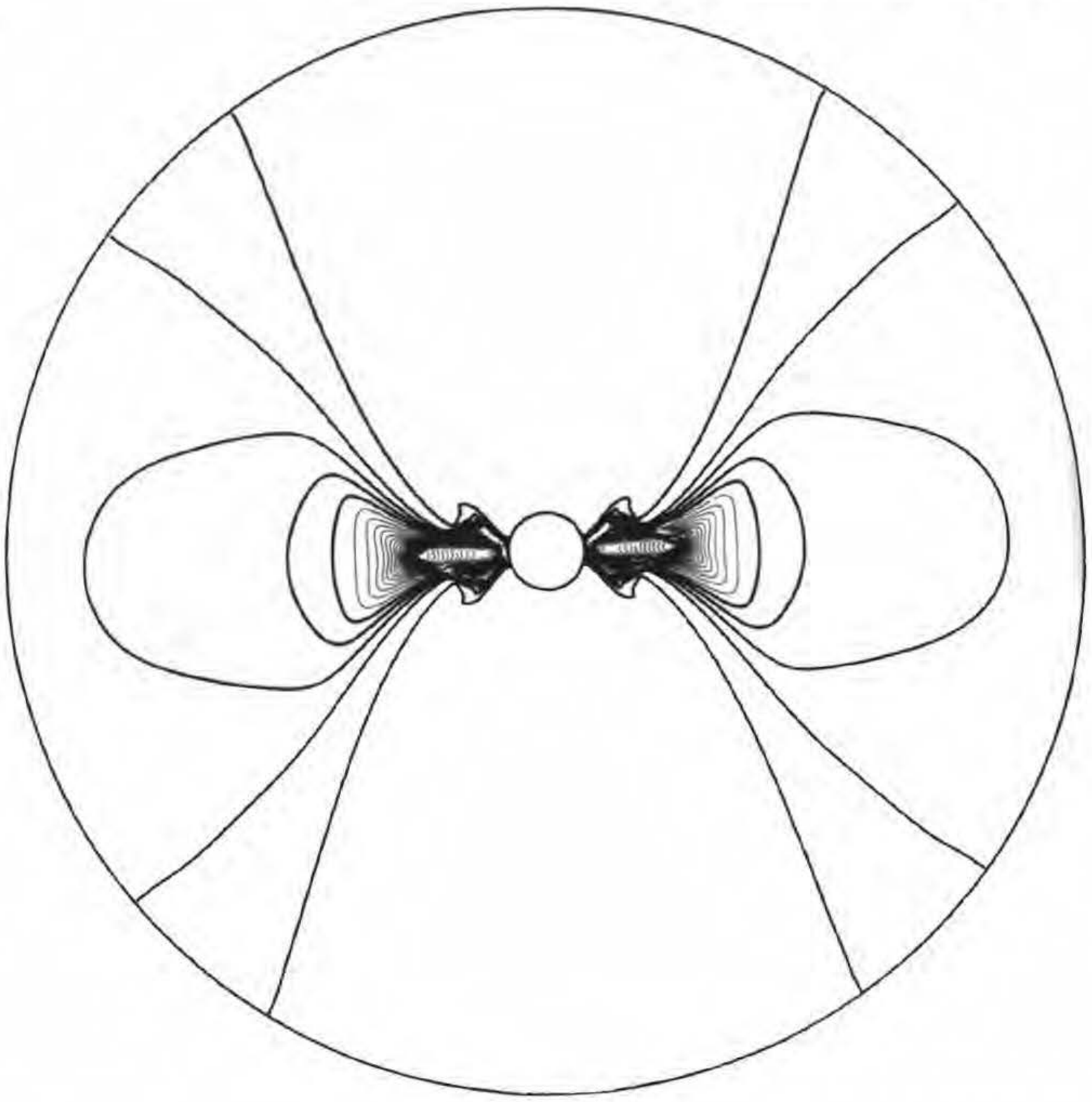


Figure three: Linear density contours showing equatorial shock at time t = 124 M for the high resolution disk formation calculation

Initially this problem was run on a grid with 30 radial and 40 angular zones using a VAX 11/780 computer. The outer boundary of the grid was at r = 27.8 M. The angular zones ran from $\theta = 0$ to $\theta = \pi$. We did not assume equatorial reflection symmetry; the equatorial zone was handled numerically in exactly the same manner as any other zone. Using the speed of light as the Courant limiter, the timestep was set to $\Delta t = 0.430$ M.

The evolutionary sequence is displayed in a series of figures. Initially the fluid falls radially onto the grid. By time t = 130 M (figure one) some fluid is down in the near hole region inside the potential cusp. There is sufficient V^{θ} velocity such that the fluid must be deflected at the equator and redirected towards the hole. By time t = 172 M backflow has

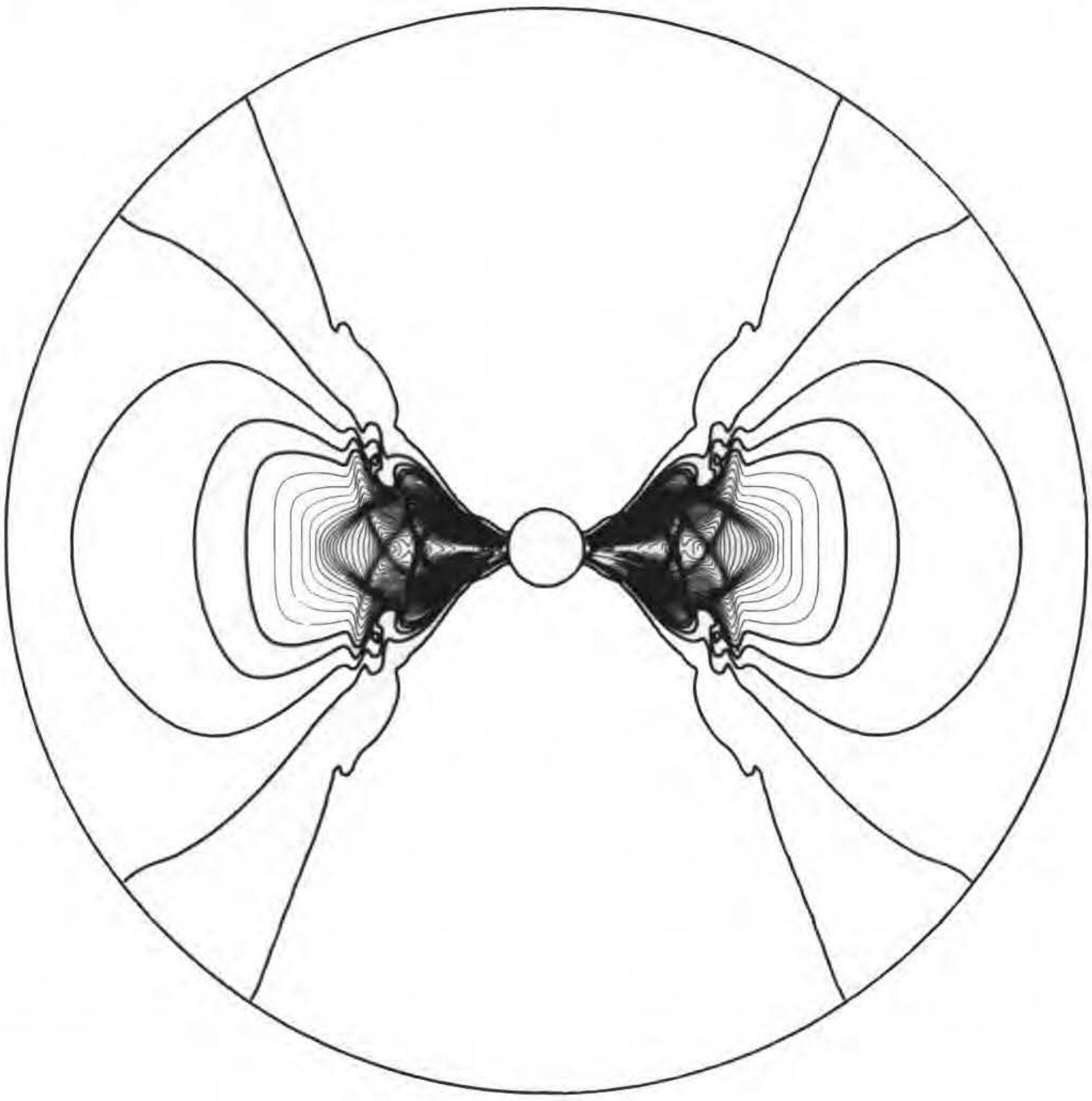


Figure Four: Linear density plots showing three pairs of shocks at time t = 180 M for the high resolution disk formation calculation.

developed along the surface of the disk accompanied by a shock. Vortices have developed at the leading edge of the backflow. As the evolution continues it becomes evident that there is a fully developed shock wave moving back through the grid with considerable outflow of fluid along the outer edges of the disk. Inflow continues along the equator. By time t = 430 M (figure two) the shock has gone off the outer boundary, cutting off fluid inflow and ending the evolution.

Comparing the state of the disk at this time with our analytic expectations reveals similarities in overall structure and some differences in details. The pressure maximum does not occur at exactly the same location as in the static disk. The temperature (and hence h) at the pressure maximum is greater than

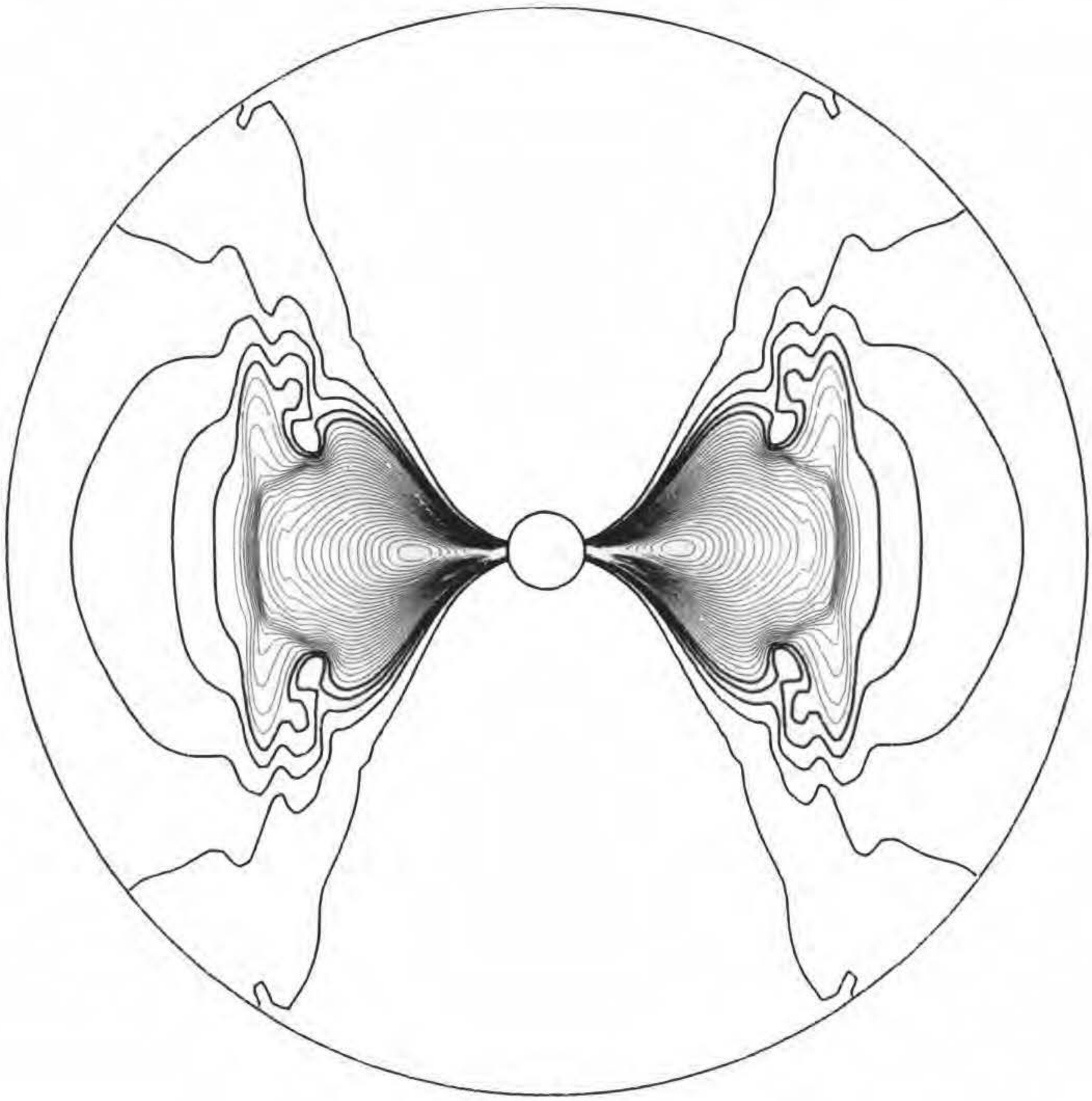


Figure Five: Linear density plot at time t = 300 M for high resolution disk formation calculation.

the static analytic value by 0.8%. Since the specific angular momentum hU_ϕ is conserved (and equal to 3.77) this means that the value of U_ϕ is reduced by the same amount. As U_ϕ determines the Keplerian orbit and the location of the pressure maximum, we find that as a result of the dynamic heating in the disk the location of the pressure maximum is moved in closer to the hole from r = 8.0 M to about r = 7.6 M. This additional heat is provided in part by the shocks which have occured and from the fact that the fluid is sent onto the grid with a significant inward velocity. Our result is consistent with the analytic value of r = 7.68 M obtained assuming a 0.8% increase in h. In this coarse grid run we have zones at r = 7.08, 7.78 and 8.54 M and have interpolated to obtain a pressure maximum location. Thus the code has found the new Keplerian orbit to the accuracy permitted by this grid.

The disk formation test model is suggestive of new dynamic phenomenon such as shocks and vortices in near black hole accretion flows. The resolution possible on this coarse a grid, however, is insufficient to study these new features in any detail. In an attempt to gain a better appreciation of the new phenomenology possible in dynamic fluid infall into a black hole we have repeated this test run using a grid with 120 radial zones, 160 angular zones and the same outer boundary (four times the resolution of the previous run). The reduction in grid size brings a corresponding reduction in the Courant-limited timestep to $\Delta t = 0.103$ M; this means that to perform the equivalent calculation requires 64 times as many computations as in the coarse grid model. Such requirements mean that while it may be feasible to run coarse grid runs on a small computer, detailed fine grid runs necessitate the use of high speed vector supercomputers. The 120 x 160 zone run we describe below was computed on the CRAY-1 supercomputer at the Max Planck Institute for Physics and Astrophysics in Garching b. Munich, West Germany. Using this machine we decreased execution time per grid point over the VAX 11/780 by a factor of about 200. In other words, this run, which required about one-half hour CPU on the Cray, would require four days CPU on a VAX.

The high resolution run reveals that while we have an overall picture of what occurs in this model, the coarse grid has failed to resolve many significant details. The difference between the two runs is most striking. The initially infalling material flows almost radially towards a point just inside r = 4 M on the equator. Here two oblique shocks form, turning the flow towards the hole (figure three). These shocks move outward and increase their angle with respect to the equator. Inside of these shocks the fluid continues to flow inward but encounters the centrifugal barrier extending out from the hole and away from the equator. This barrier defines the so-called "funnel" (12), the region along the orbital axis which is kept evacuated by centrifugal accelerations. Fluid encountering this centrifugal barrier slows and stops; material begins to pile up behind and two curved shocks form, moving out and away from the centrifugal barrier. Behind these shocks the fluid above and below the equator has turned in its orbit and flows outward until reaching the infalling fluid. Here it is turned again to flow up along the surface of the infalling disk. Two additional curved shocks result from this collision (figure four). Along the leading edge of the backflow, shear instabilities produce a vortex. All these features have formed by time t = 180 M. By this time in the low resolution run there was observable backflow and a shock had occured but the three seperate shock features were not resolved. The vortices were apparent in the coarse grid run; what had produced these vortices was less clear.

The shocks continue to move outward through the infalling fluid until, by the end of this calculation at time t = 300 M,

they have run together (figure five). After the infall, the splash off the centrifugal wall and the outward traveling shocks, the fluid is relaxing towards a hot, pressure supported fat disk. A particularly significant feature revealed by this high resolution calculation is that complicated hydrodynamics can occur inside of r = 6 M, the marginally stable orbit. This is contrary to expectations based upon the usual one dimensional thin disk model. This near hole physics is especially important inasmuch as the most energetic phenomenon will occur in the deepest part of the potential.

This calculation is but one example of the new physical phenomena which our numerical approach is bringing to light. Through this work we hope to establish the foundation for extensive investigations into the physics of accretion into black holes. Our results will add to the detailed understanding of the central engines of many of the most intriguing astrophysical object.

6. SUMMARY

To conclude we note that while we have presented our work as a study of black hole accretion, it has a broader context. For example, these techniques can be applied to other problems, including the matter-coupled Einstein equations. In a code to solve those equations our work would become just a subroutine! More generally, our work to date can be viewed as establishing a paradigm for code calibration. Concurrent with the present development of supercomputers, there is increasing interest in the numerical approach to complicated astrophysical problems previously considered unsolvable. It is vital to calibrate and document one's numerical tools as a prerequisite for the presentation of results. The analogy with experimental sciences is obvious. The future will see the acceptance of numerical techniques as a primary tool for the theorist's investigation of the complex equations of relativity.

7. ACKNOWLEDGEMENTS

This work has been supported by NSF grants PHY80-01496 and PHY83-08826. LLS wishes to acknowledge receipt of an Alfred P. Sloan Fellowship. We wish to thank Prof. Kippenhahn and the Max Planck Institute for Physics and Astrophysics for generously allowing us the use of the Insitute Cray computer as well as providing support during our visit in 1983. The tireless and patient help of Karl-Heinz Winkler and Michael Norman with the Munacolor graphics routines was essential for our completion of this project and their efforts are gratefully acknowledged. JFH wishes to thank Dr. Martin Rees, Dr. Lynden-Bell and the Institute

of Astronomy, Cambridge for their hospitality during his visits. Finally, we wish to thank Joan Centrella, Michael Norman and Karl-Heinz Winkler for many illuminating discussions.

REFERENCES

1. Hawley, J. F., Smarr, L. L., and Wilson, J. R. 1984, Ap. J., 277, in press.

2. Hawley, J. F., Smarr, L. L., and Wilson, J. R. 1984, preprint IAP 83-13, to appear in Ap. J. Suppl.

3. Smarr, L. L., Taubes, C., and Wilson, J. R. 1980, from "Essays in General Relativity," ed. F. J. Tipler (New York: Academic Press).

4. York, J. W. 1978, from "Sources of Gravitational Radiation," ed. L. Smarr (New York: Cambridge).

5. Wilson, J. R. 1978, in "Proceedings of Inst. Sch. of Phys. Fermi Course LXV," (Amsterdam: North Holland).

6. Norman, M. L. and Winkler, K.-H. 1984, in "Astrophysical Radiation Hydrodynamics," ed. M. L. Norman and K.-H. Winkler (Dordrecht: Reidel), in press.

7. Wilson, J. R. 1972, Ap. J., 173, pp. 431-438.

8. Von Neumann, J. and Richtmyer, R. D. 1950, J. Appl. Phys., 21, pp. 232-237.

9. Sod, G. A. 1978, J. Comp. Phys., 27, pp. 1-31.

10. Van Leer, B. 1977, J. Comp. Phys., 23, pp. 276-299.

11. Centrella J. and Wilson, J. R. 1983, preprint IAP 83-11, submitted to Ap. J.

12. Lynden-Bell, D. 1977, Phys. Scripta, 17, pp. 185-191.